Thin Solid Films 789 (2024) 140196

Contents lists available at ScienceDirect

Thin Solid Films

journal homepage: www.elsevier.com/locate/tsf

Admittance spectroscopy study of defects in β-Ga_2O_3

Jian V. Li [a,b,*], Jessica Hendricks [a,c], Adam Charnas [a], Brenton A. Noesges [a,b], Adam T. Neal [a], Thaddeus J. Asel [a], Yunjo Kim [a], Shin Mou [a]

[a] Air Force Research Laboratory, Materials and Manufacturing Directorate, Wright-Patterson AFB, OH 45433, USA
[b] Azimuth Corporation, Beavercreek, OH 45324, USA
[c] UES Corporation, Beavercreek, OH 45432, USA

ARTICLE INFO

Keywords:
Gallium oxide
Defect
Mobility
Admittance spectroscopy
Schottky

ABSTRACT

We present a comprehensive investigation of electrically active defects and transport properties in commercial ($\bar{2}$01) edge edge-defined film-fed growth β-Ga_2O_3 using admittance spectroscopy measurements from 14 K up to 450 K. Isothermal capacitance-frequency measurements were conducted from 410 to 450 K to resolve a defect ~0.8 eV below the conduction band edge and compared with deep-level transient spectroscopy and isothermal capacitance transient spectroscopy measurements. We report significant non-Arrhenius behavior of a defect ~100 meV below the conduction band and apply the Arrhenius transformation matching method to extract its temperature-dependent activation energy and capture cross-section in the temperature range of 75 to 195 K. At low temperatures (<50 K), we use bias-dependent admittance spectroscopy to extract the electron mobility in β-Ga_2O_3 from the modified dielectric relaxation frequency. Finally, we discuss the potential of admittance spectroscopy for defect characterization in wide bandgap semiconductors in terms of the defect detection range, instrument requirements, and the frequency-temperature experiment space.

1. Introduction and motivation

The commercial viability of β-Ga_2O_3-based power electronics technology [1,2] depends on comprehensive and in-depth understanding of point and extended defects [3] in this ultra wide bandgap semiconductor material [4,5], which is only achievable through thorough and reliable characterization. Because of their choices of stimuli and responses, electrical characterization methods are the most revealing of defect behavior relevant to device operation. Prominent examples of electrical characterization techniques are deep-level transient spectroscopy (DLTS) [6] and its variant deep-level optical spectroscopy (DLOS) [7], which are suitable for the wide bandgap semiconductors and have achieved great success in β-Ga_2O_3 [8,9]. This work presents a study of defects in β-Ga_2O_3 using admittance spectroscopy, which both corroborates and complements DLTS/DLOS techniques.

In this work we limit the scope to thermal, i.e., non-optical admittance spectroscopy [10], which is a member of the semiconductor-junction based capacitance technique suite that also includes capacitance-voltage carrier density profiling and DLTS. Admittance is used to the device under test with the equivalent circuit of a capacitor and conductance connected in parallel, which are respectively measured from the quadrature and in-phase current responses to small AC voltage modulation. In the most basic device model, i.e., a single-sided depletion region sandwiched by infinitely conductive quasi-neutral regions with perfect Ohmic-contacts, the admittance signals originate from the charge response of majority-carrier trapping defects in the depletion region. The thermal activation of this process is spectroscopically manifested in the frequency and temperature dependence of the admittance, which allows the extraction of the activation energy E_a, capture cross-section σ_n, and density N_t or density of states $N_t(E)$ [11] of the defect. Other physical mechanisms beyond the above basic model may contribute to the admittance spectroscopy measurement and, when discerned by additional measurements (e.g., bias voltage dependence) and interpreted with suitable models, allow the extraction of related information such as carrier mobility [12] and non-Ohmic contact barrier height [13].

In this work, we present the use of admittance spectroscopy for studying defects in β-Ga_2O_3 materials. Under certain conditions and using an appropriate model, we also use admittance spectroscopy to investigate electron mobility in β-Ga_2O_3. We discuss the range of defect detection using admittance spectroscopy and options to extend this range for wide bandgap semiconductors.

* Corresponding author.
E-mail address: jian.li.1.ctr@us.af.mil (J.V. Li).

https://doi.org/10.1016/j.tsf.2023.140196
Received 17 July 2023; Received in revised form 10 November 2023; Accepted 29 December 2023
Available online 30 December 2023
0040-6090/Published by Elsevier B.V.

2. Experiment

The material studied in this work is ($\bar{2}$01) unintentionally doped (UID) n-type β-Ga_2O_3 substrates grown by the edge-defined film-fed growth method by Tamura Corporation, Japan before its spin-off into Novel Crystal Technology. The substrates have one chemically-mechanically polished surface (top side) and one as-lapped surface (bottom side). Ohmic contacts were formed by sputtering deposition of a 50 nm/1000 nm Ti/Au metal layer to the bottom following solvent cleaning. The Ohmic-contacted samples were annealed in a tube furnace with Ar gas flow using a 15-minute ramp from room temperature to 450 °C to improve the contact resistance. We then formed Schottky contacts by sputtering deposition of a 150 nm Au metal layer in circular patterns with 300 μm diameters on the top side with no further intentional annealing. The finished samples were mounted to the QFP44 ceramic package through silver paste and individual devices wire bonded through the top Schottky contacts.

We used a Keysight E4990A impedance analyzer (also called an inductance-capacitance-resistance, LCR, meter) for the AS measurements with an AC modulation voltage of 50 mV_{pp} in the frequency range from 20 Hz to 3 MHz and a DC bias voltage in the range of +0.5 to −5.0 V. The low-frequency noise was significant at frequencies below 1 kHz, hence a 16-point averaging was applied. The effect of a two-meter long cable over the operation frequency range was taken into account through phase and load calibration. The temperature of the sample was controlled by a closed-cycle helium-cooled cryostat capable of stabilizing the temperature at any set point between 14 and 800 K. Experimental data included in this work were however limited to 450 K due to the melting point of $Sn_{0.63}Pb_{0.37}$ solder used in parts of the cabling. The doping profile was calculated to be a constant 1.27×10^{17} cm^{-3} from capacitance-voltage measurement conducted at $f = 100$ kHz and room temperature in a DC bias range from +0.5 to −1.5 V. The isothermal capacitance transient spectroscopy (ICTS) measurement [14] was carried out using the same impedance analyzer at a fixed frequency of 100 kHz and after the DC bias voltage was held at +0.5 V for 60 s and then switched to −6.0 V at zero time.

3. Results

We first measured the capacitance while sweeping the AC modulation frequency from 20 Hz to 200 kHz (Fig. 1a) with the sample temperature varied between 410 and 450 K. The capacitance plateaued on the low frequency end of the spectrum up to ~100 Hz before it transitioned downward to a baseline above ~10 kHz. The phase angle of the capacitance measurement was higher than 50° throughout the above frequency range. The high-to-low step transition of capacitance signifies a possible defect, the inflection frequency of the capacitance transition $f_{pk} = \omega_{pk}/2\pi$ being associated with the emission rate of the defect e_n (i.e., the inverse of the emission time τ) at certain temperature T according to [15]

$$\omega_{pk} = e_n = 1/\tau = \nu_0 \times \exp(-E_a / kT), \quad (1)$$

where E_a and ν_0 are the activation energy and attempt-to-escape frequency of the electron's emissive excitation from the defect to the conduction band, respectively, and k the Boltzmann's constant. As shown in Fig. 1a, the differential capacitance spectrum $f \times dC/df$ exhibited a (negative) peak at f_{pk}, which was used for more accurate measurement of the inflection frequency than the raw capacitance-frequency spectrum. The capacitance-frequency spectra measured at progressive decreasing temperatures exhibited the expected red-shift behavior of f_{pk}. An Arrhenius plot (Fig. 1c) was constructed from the temperature-dependent ω_{pk} data to extract $E_a = 0.754$ eV and capture cross-section $\sigma_n = 6.84 \times 10^{-15}$ cm^2, taking into account that $\nu_0 = N_c \times \nu_t \times \sigma_n$, where N_c (3.7×10^{18} cm^{-3}) is the effective density of states of the conduction band and ν_t (1.0×10^7 cm/s) the thermal velocity of

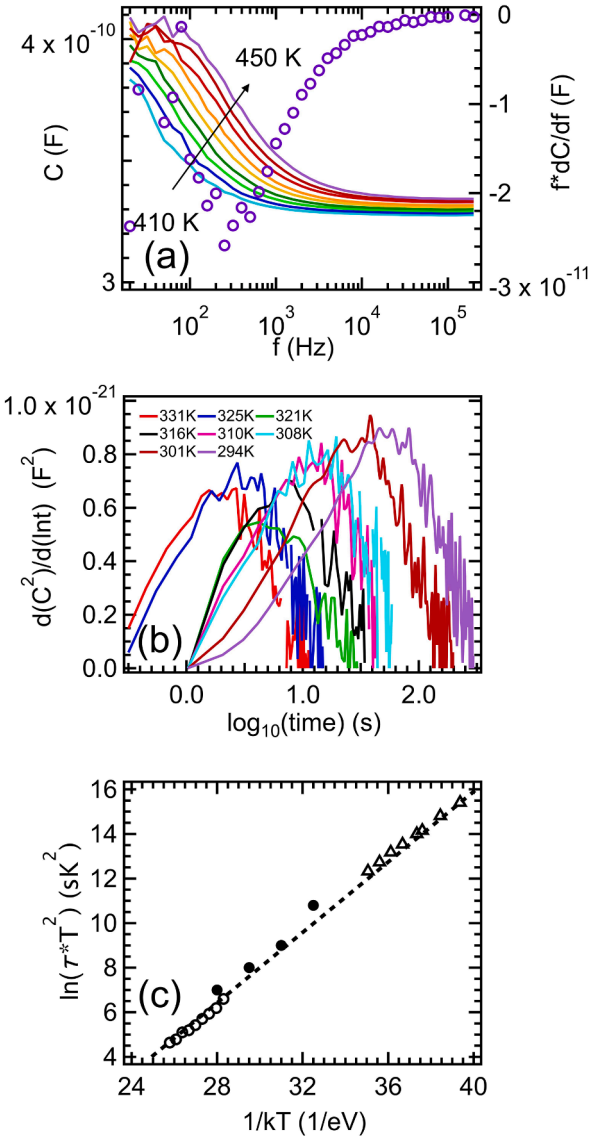

Fig. 1. (a) Raw capacitance (C vs f, lines) spectra measured at zero bias and at temperatures between 410 and 450 K in 5 K steps and the differential capacitance ($f \times dC/df$ vs f, symbols) spectrum at $T = 450$ K; (b) ICTS spectra recorded after the bias voltage is switched to −6.0 V between 294 and 331 K; and (c) Arrhenius plots constructed from AS (open circles) and ICTS (open triangles) spectra in (a) and (b) alongside DLTS (filled circles) data reproduced from Ref. [9].

electrons. The density of this defect is extracted as $N_t = N_d \times (\Delta C \times \lambda)/(C_\infty \times W) = 2.07 \times 10^{16}$ cm^{-3}, where $\Delta C = 7.09 \times 10^{-11}$ F is the magnitude of the high-to-low capacitance step, $C_\infty = 3.34 \times 10^{-10}$ F the baseline capacitance at high frequency, $\lambda = 79.1$ nm the crossing point of the defect level and Fermi level measured from the depletion region boundary, and $W = 103$ nm the depletion width.

We also conducted ICTS measurement at a lower temperature of 294 to 331 K to detect thermally-activated defect emission behavior (Fig. 1b). The Arrhenius plot (Fig. 1c) constructed from the temperature dependent ICTS data lines up with that from the admittance spectroscopy data. The extracted activation energy $E_a = 0.714$ eV and capture cross-section $\sigma_n = 7.89 \times 10^{-16}$ cm^2 agree well with those measured by admittance spectroscopy earlier, both being in close agreement with previous DLTS measurements of the well-known defect located at ~0.8 eV below the conduction band, sometimes referred to as the E_2 defect [8,9,16,17]. The gap between the two Arrhenius plots in Fig. 1b is

inaccessible to either AS or ICTS due to instrumentation limits but is well covered by DLTS, as demonstrated using data points reproduced from Zhang et al. [9]. This defect is commonly believed to originate from either Fe [16] or V_{Ga} related complex [17], which sees a major role in compensation doping and semi-insulating substrate. Polyakov et al. used temperature-dependent capacitance at various frequencies to observe the Fe-related defect at ~0.8 eV [18] and later a defect ~1.0 eV [19] below the conduction band. The consistency between AS, ICTS, and DLTS data establishes the validity and corroborative value of AS measurement of majority carrier trapping defects.

Lowering the temperature to below 200 K allows another AS signature to be observed. Raw and differential capacitance spectra from 195 to 75 K are shown in Fig. 2a and 2b, respectively. The Arrhenius plot constructed from peaks of the differential capacitance spectra measured between 65 and 235 K is shown in Fig. 2c. From 235 to ~ 150 K (i.e., $1/kT < 80$ eV^{-1} in Fig. 2c), the thermal activation of the AS signature is Arrhenius, enabling extraction of $E_a = 93.6$ meV and $\sigma_n = 3.14 \times 10^{-18}$ cm^2. Results based on the Arrhenius behavior of this defect was first reported by Neal et al. [20] and later confirmed by Ghadi et al. [21]. However, for $T < 150$ K (i.e., $1/kT > 80$ eV^{-1} in Fig. 2c), the thermal activation behavior exhibits substantial non-Arrhenius features, rendering a non-linear "Arrhenius plot". A non-linear Arrhenius plot indicates temperature dependent E_a and or ν_0 which invalidates the underlying assumption of the linear fitting procedure and prevents reliable extraction of both parameters over a wide temperature range. This non-Arrhenius behavior had been observed in a large amount of substrate and epitaxial samples [22].

Conventional admittance spectroscopy as described earlier is based on isothermal measurements of admittance in the frequency domain, which in essence scans the emission rate ν while keeping the temperature T constant. Considering the temperature-rate duality, we obtained the alternative isorate measurements where T is scanned with ν fixed (indicated by the vertical dashed line in Fig. 2b) and applied the Arrhenius-transformation-matching method (ATM) [23] to the isothermal and isorate spectra to extract E_a and ν_0. We used the T-E_a transformation

$$E_{a,T} = kT \times \ln(\nu_0 / \nu_{fix}) \quad (2)$$

to transform T to $E_{a,T}$ and ν-E_a transformation

$$E_{a,\nu} = kT_{fix} \times \ln(\nu_0 / \nu) \quad (3)$$

to transform ν to $E_{a,\nu}$, which produces the virtual scans of $f \times dC/df(E_{a,T})$ and $f \times dC/df(E_{a,\nu})$ in the activation energy space from the experimentally obtained isothermal scan $f \times dC/df(\nu)$ and isorate scan $f \times dC/df(T)$, respectively. Since the two experimental scans $f \times dC/df(\nu)$ and $f \times dC/df(T)$ probe the activation behavior of the same thermally activation process, the corresponding virtual scans $f \times dC/df(E_{a,\nu})$ and $f \times dC/df(E_{a,T})$ should agree with each other, such as demonstrated in Fig. 3a, if and only if the T-E_a and ν-E_a transformations uses the ν_0 value true to the thermal activation process physically responsible to both scans. Once ν_0 is thus determined, E_a is computed by Eq. (1) since E_a and ν_0 together satisfy Eq. (1) at (T_{fix}, ν_{fix}). The above procedure can be carried out in a small temperature-rate range to extract E_a and ν_0 local to that T-ν space. In Fig. 3b we show that $E_a(T)$ and $\nu_0(T)$ exhibit a strong dependence on

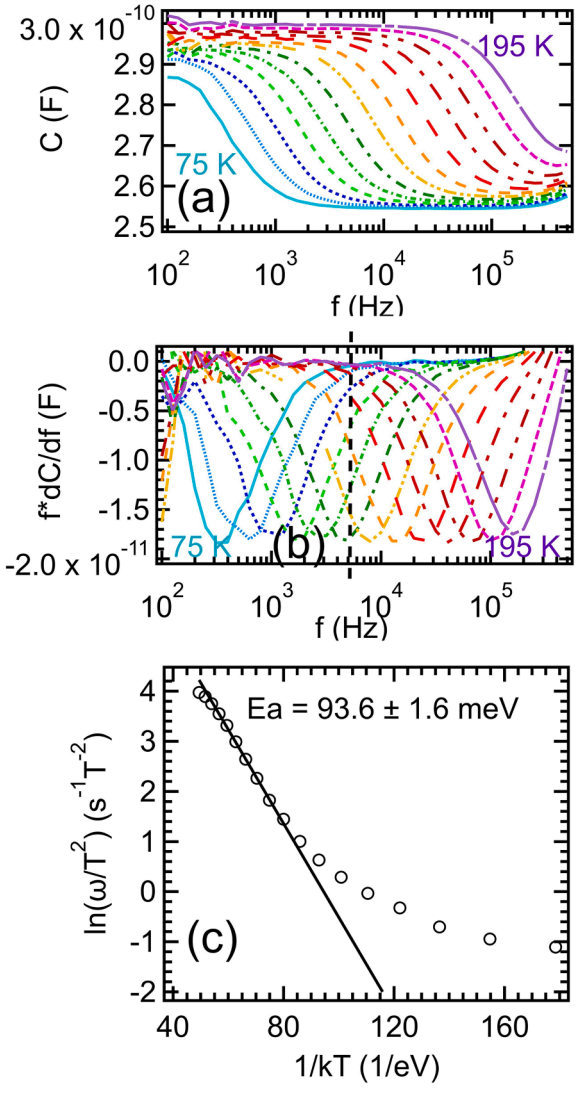

Fig. 2. (a) Raw capacitance spectra, (b) differential capacitance spectra measured at zero bias between 75 and 195 K, and (c) the resultant Arrhenius plot constructed from peaks measured between 65 and 235 K including those in (b).

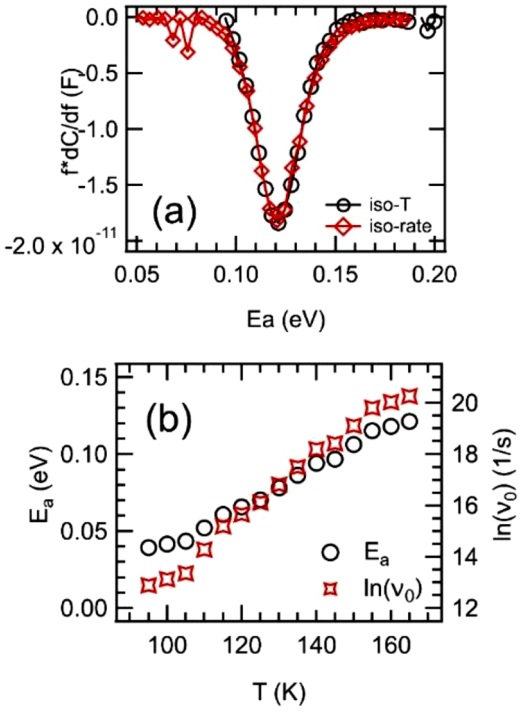

Fig. 3. (a) Matching of isothermal (diamonds, measured at 165 K) and isorate (circles, measured at 31,622 s^{-1}) differential capacitance spectra when $\nu_0 = 6.31 \times 10^8$ s^{-1} is used in Eqs. (2) and (3) to match the two virtual scans and extract $E_a = 121$ meV, and (b) E_a and ν_0 determined by the ATM method at various temperatures.

temperature. The capture cross section increases almost exponentially with temperature suggesting that multi-phonon emission [24] is the more probable capture mechanism than other candidates such as radiative, Auger, and cascade mechanisms.

Next we lowered the sample temperature even further to below 30 K where the capacitance measured at 1 MHz and zero bias (Fig. 4a) rapidly changed near ~30 K, indicating the presence of another AS signature. Differential capacitance spectra taken at 0 V and various temperatures (Fig. 4b) indeed reveal prominent peaks, from which an Arrhenius plot was constructed (Fig. 4c) and used to extract an activation energy E_a ~ 11 meV neglecting non-Arrhenius characteristics at lower temperatures. This small activation energy is close to the ionization energy of Si dopants measured by Hall method [16] and temperature-dependent capacitance measurements [25], which could be one of the species contributing to the unintentional doping. Within the frequency range of the impedance analyzer used in this study, this AS signature was only observed at very low temperatures. The effective depletion width measured at 1 MHz and zero bias (Fig. 4a) drastically increased from ~100 nm to several μm as the temperature dropped below 30 K, which is not explainable by an ideal Schottky junction model (note that the smaller step near 250 K corresponds to the ~100 meV defect discussed above) even with the inclusion of a secondary junction (such as a non-Ohmic contact) and requires the inclusion of freeze-out effect of carrier density or mobility.

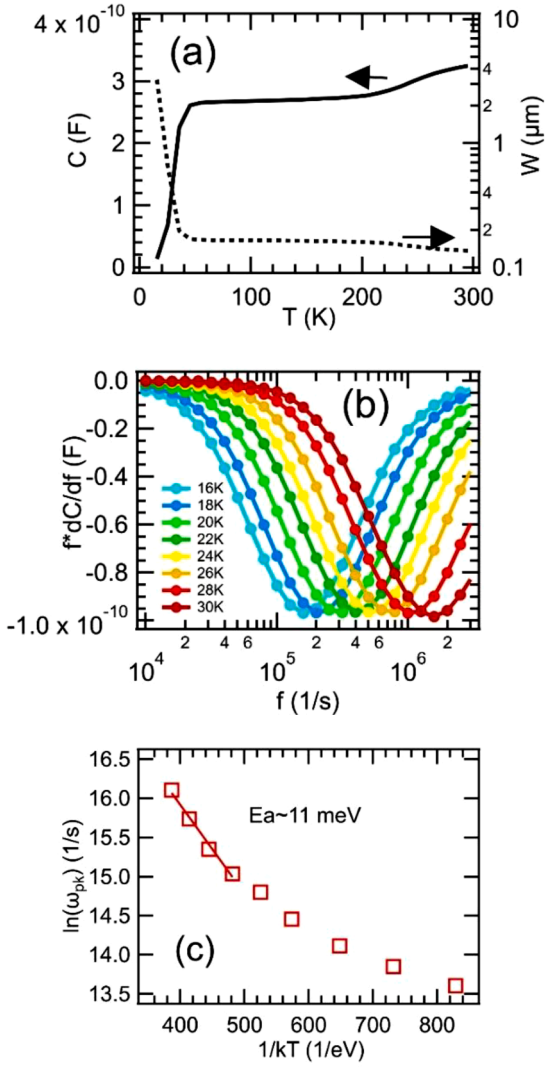

Fig. 4. (a) The temperature dependence of capacitance (solid line) and depletion width (dotted line) measured at 1 MHz and zero bias, (b) differential capacitance spectra measured between 16 and 30 K at zero bias, and (c) the Arrhenius plot constructed from peaks in (b).

Indeed, the peak observed in Fig. 4a is due to dielectric relaxation of the quasi-neutral Ga_2O_3 part of the device. An un-depleted (neutral) bulk semiconductor characterized by resistivity ρ and permittivity ε exhibits dielectric relaxation [26] at frequency $\omega_{dr} = 1/\rho\varepsilon$. Below ω_{dr}, the semiconductor behaves as a geometrically defined conductor with $G_g = A/\rho t$, where A is the contact area and t is the thickness. Above ω_{dr}, the semiconductor behaves as a geometrically defined capacitor $C_g = \varepsilon A/t$. The complete equivalent circuit of the quasi-neutral Ga_2O_3 is therefore the parallel combination of C_g and G_g. In the presence of the Schottky junction (Fig. 2), the depletion capacitance is additionally connected in series with the sub-circuit of the quasi-neutral Ga_2O_3. As a result, the inflection frequency observed by admittance spectroscopy is the dielectric relaxation frequency of the quasi-neutral Ga_2O_3 modified by a factor of W/t. Because W varies with bias voltage, the modified dielectric relaxation frequency becomes bias dependent (Fig. 5a) according to [27]:

$$\omega_p^2 = \frac{W^2}{t^2\rho^2\varepsilon^2} = \frac{2}{q\varepsilon N_d\rho^2 t^2}(V_{bi} - V), \tag{4}$$

where V_{bi} is built-in potential of the Schottky junction. After the carrier concentration N_d is determined from capacitance-voltage (CV) measurement, one plots ω_p^2 against bias V (Fig. 5b) and uses the slope of this plot to determine the resistivity or mobility. At 24 K, we determined the electron mobility of the Ga_2O_3 sample as ~1 $cm^2/V/s$. Fig. 5c shows the temperature-dependent electron density N_d measured at 10 kHz and mobility μ (circles) extracted according to Eq. (4) from 16 to 28 K.

4. Discussions

The span of the two-dimensional frequency-temperature space reachable by any admittance spectroscopy experiment determines [28] the range of defects detectable, which is important for the increasingly active research of wide bandgap semiconductor materials. Because the activation energy E_a corresponds approximately to the energetic location of defects in the bandgap, it is a convenient and practical metric for defect detection range. Obviously, the assessment of defect detection range is only quantitatively determined when the variation of the capture cross-section is fully factored in. For the qualitative discussion below aiming at a rough quantitative guidance, we limit the variability of capture cross-section to the values experimentally extracted from this work earlier. Even assuming a fixed capture cross-section, it is immediately clear (Fig. 6) that the thermal activation nature of charge exchange with defects in wide bandgap semiconductors demands admittance spectroscopy measurement spanning several decades in temperature and even more in frequency. As illustrated in Fig. 6, the most often seen AS system is based on an LCR meter or an impedance analyzer for a frequency range of 10 – 10^6 Hz and a liquid-nitrogen cooled cryostat for a temperature range of 80 to 350 K. The frequency-temperature window of this baseline configuration is barely capable of detecting E_a between 0.1 and 1.0 eV.

An energy range between 0.1 and 1.0 eV is insufficient for studying defects in wide bandgap semiconductors. The frequency-temperature window of the baseline AS configuration overlaps only with the low-rate portion of typical DLTS experiment space, which explains its relative disadvantage on the high-E_a side and slight advantage on the low-E_a side. An RF network analyzer (NA) can be employed to extend the high-frequency end by 3~4 decades provided that additional requirements of device fabrication, probe/cable assembly, and calibration are met. On the low-frequency end, one can use a lock-in amplifier (LIA) to gain an additional 3~4 decades. ICTS [29], often using the same baseline instrument of LCR meter or impedance analyzer, is perhaps the most economical and feasible route to extend the frequency range. It has the

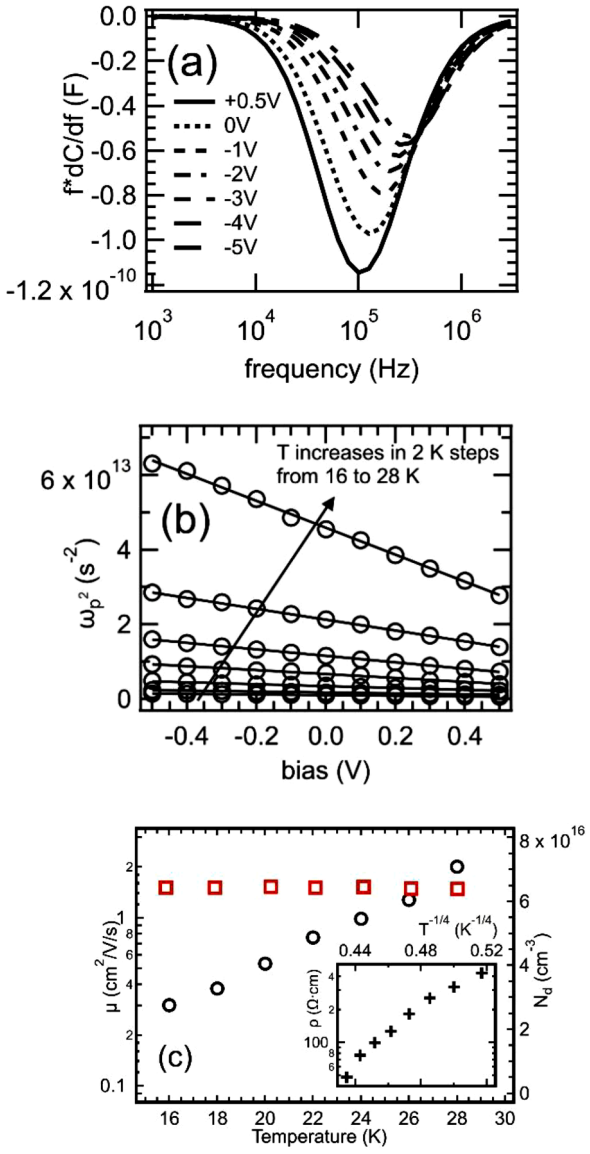

Fig. 5. (a) Differential capacitance spectra measured between 1 kHz and 3 MHz at 14 K when varying the DC bias voltage from +0.5 V to −5.0 V showing a red shift in the peak position with increasing forward bias consistent with the modified dielectric relaxation interpretation; (b) the bias dependence of the squared peak positions of the differential capacitance spectra at temperatures from 16 to 28 K, with a finer voltage step size than (a) to facilitate the linear fitting; (c) the temperature dependence of electron density N_d (squares) measured at 10 kHz and mobility μ (circles) extracted according to Eq. (4) and; inset: log(ρ) exhibit reasonably linear dependence on $T^{-1/4}$.

advantage of being measured at a fixed medium-to-high frequency thus circumventing the low-frequency noise challenge faced by impedance analyzers. The short-time limit of ICTS is set by the instrument to ~100 ms whereas its long-time end is limited by practicality to ~10^5 s (1 day). Closed-cycle or constant-flow helium cooling extends the low temperature limit to ~10 K, provided that the Ohmic contact and conductivity of the quasi-neutral region do not pose problems at this temperature. This low-temperature extension, especially in combination with high-frequency extension enabled by a network analyzer, lowers the low-E_a limit to ~10 meV. A high-temperature cryostat may reach 800 K which can raise the high-E_a limit to 2.0 eV, especially when combined with long-time operation of ICTS.

It is thus apparent that thermal admittance spectroscopy can in principle achieve a range of ~10 meV to ~2.0 eV, which sufficiently

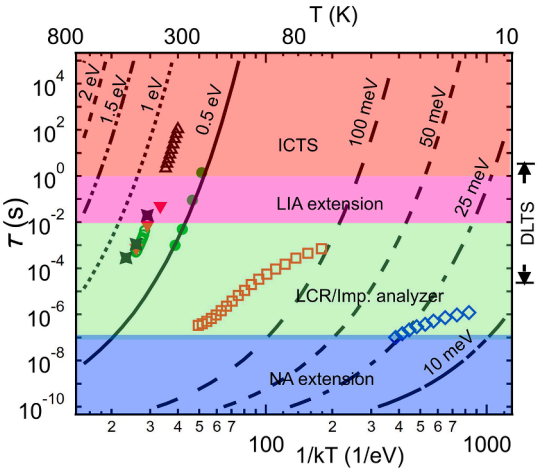

Fig. 6. Presentation of the time-temperature space for admittance spectroscopy experiment showing detection of defects in Figs. 1, 2, & 4 of this work (open circles: 0.8 eV, admittance spectroscopy; open triangles: 0.8 eV, ICTS; open squares: 100 meV; open diamonds: freezeout), experimental data reproduced from Ref. [8] (filled circles, 0.6 eV; filled triangles, 0.8 eV, filled stars, 1.0 eV), and hypothetical defects (lines, assuming various E_a with fixed $\nu_0 = 2.53 \times 10^{11}$ s^{-1} in Eq. (1)). Colored rectangles approximately represent the typical scope of time-temperature space achieved by an LCR meter or an impedance analyzer (green) and extensions of which enabled by a network analyzer (NA, blue), a lock-in amplifier (LIA, cyan) and the ICTS technique (orange).

covers half of the bandgap of most today's wide bandgap semiconductors including SiC, GaN, and β-Ga_2O_3. Since thermal admittance spectroscopy is sensitive to majority carrier change with defects, the entire bandgap can be inspected by combining the top half with an n-type sample and the lower half with a p-type sample, provided that both types of doping are feasible. In the case of β-Ga_2O_3 where p-type doping is currently not yet realized, one may resort to optical excitation to implement optical admittance spectroscopy [30], similar to DLOS, to probe the entire bandgap. Because the carrier-defect exchange rate under optical excitation is directly proportional to the optical flux of applicable photons, the optical transition rate can be made much higher than the thermal rate, thus enabling detection of high transition energy within the same temperature-frequency window. On the other hand, the thermal admittance spectroscopy signature of a defect provides valuable perspective on its role for specific devices. For example, the capture/emission rate of the 0.8 eV defect at 600 K is ~10^6 1/s, which may have some bearing on power electronic (PE) or even RF devices operating at high temperatures, especially considering the effects of local heating and constrained thermal conduction.

Because admittance spectroscopy is a steady-state small-perturbation measurement, as opposed to large-perturbation transient techniques such as DLTS and ICTS, it can be naturally used in conjunction with other steady-state measurements, in particular CV carrier density profiling. Fig. 7 shows the carrier density profiles extracted from CV measurements conducted at 195 K and several frequencies strategically located on both sides of the inflection frequency in Figs. 2(a) and 2(b) due to the trap with $E_a = 93.6$ meV. At a frequency sufficiently below the inflection frequency, the measured capacitance includes dynamic charge response from the trap, which is opposite of the case above the inflection frequency. The difference between the carrier density profiles extracted at these two frequencies reveals the depth distribution of the trap (Fig. 7) detected in AS spectra. This information needs to be used with the caution because the actual depth of the responding trap is offset from the depletion region boundary W by λ [15]. Also, the traps contribute to the CV measurement electrostatically [31] even if they are not dynamically responding at the measurement frequency, pointing to more preferable methods such as drive-level capacitance profiling [31]

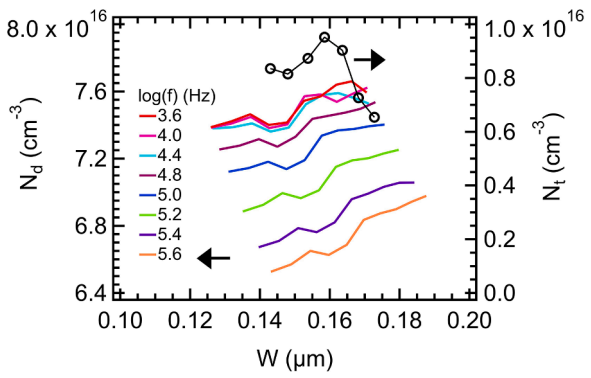

Fig. 7. The carrier density profiles (left axis, lines) extracted from capacitance-voltage measurements conducted at 195 K and various frequencies and trap density profile (right axis, circles) obtained from the difference between the carrier density profiles extracted sufficiently above ($10^{5.6}$ Hz) and below ($10^{4.8}$ Hz) the inflection frequency in the C(f) spectrum, i.e., $10^{5.2}$ Hz in Fig. 2(a).

for the purpose of profiling traps.

The electron mobility extracted at low temperatures in Fig. 5(c) qualitatively agrees with the expected dominance of transport by the ionized impurity scattering mechanism based on Hall measurement of β-Ga_2O_3 samples [20] of similar doping and growth method. There have been reports of impurity band conduction in β-Ga_2O_3 at very low temperatures [32,33]. As shown in Fig. 5(c) and its inset, the electron density remains constant for the sample studied in this work at T<30 K while the logarithmic resistivity exhibits a reasonably good linearity with respect to $T^{-1/4}$, indicating that the variable range hopping mechanism described by Shklovskii-Efros [34] likely plays an important role. This inference is supported by the observation in Fig. 4 that the activation energy of conductivity decreases with decreasing T – another signature of variable range hopping. From a methodology point of view, the AS-based method demonstrated in this work complements the Hall technique especially for high-resistivity samples because it requires only modest current and voltage biases and measures the mobility in the crystal growth (vertical) direction instead of the in-plane direction.

5. Conclusion

In summary, we demonstrated admittance spectroscopy detection and characterization of the defect located at 0.8 eV below the conduction band of β-Ga_2O_3 at relative high temperatures (>300 K), in consistency with DLTS and ICTS measurements. Significant non-Arrhenius behavior was observed in the ~100 meV defect observed by admittance spectroscopy. We used the ATM method to extract temperature-dependent activation energy and capture cross-section, the latter indicating that a multi-photon excitation process is likely responsible for the carrier capture process of this defect. At low temperatures <50 K, we used admittance spectroscopy to investigate the dielectric relaxation frequency of β-Ga_2O_3 modified by the presence of a Schottky junction. The electron mobility was extracted from 14 to 30 K. We show that thermal admittance spectroscopy, in combination with ICTS and high measurement temperature, is capable of covering an activation energy range of 0.1 to 2.0 eV with commonly used instruments.

CRediT authorship contribution statement

Jian V. Li: Conceptualization, Investigation, Formal analysis, Writing – original draft. **Jessica Hendricks:** Investigation, Writing – review & editing. **Adam Charnas:** Investigation, Writing – review & editing. **Brenton A. Noesges:** Resources. **Adam T. Neal:** Investigation, Writing – review & editing, Resources. **Thaddeus J. Asel:** Resources. **Yunjo Kim:** Investigation, Resources. **Shin Mou:** Funding acquisition, Resources, Investigation, Supervision, Writing – review & editing.

Declaration of Competing Interest

The authors declare that they have no known competing financial interests or personal relationships that could have appeared to influence the work reported in this paper.

Data availability

Data will be made available on request.

Acknowledgments

The authors acknowledge financial support from AFOSR grant 23RXCOR017 (P.O.: Dr. Ken Goretta) and OUSD (R&E) with the APEX ARAP program (P.O.: Dr. Karl Dahlhauser). This research was performed while A. Charnas held an NRC Research Associateship award at AFRL RX.

References

[1] M.J. Tadjer, Toward gallium oxide power electronics, Science 378 (2022) 724, https://doi.org/10.1126/science.add2713.
[2] A.J. Green, J. Speck, G. Xing, P. Moens, F. Allerstam, K. Gumaelius, T. Neyer, A. Arias-Purdue, V. Mehrotra, A. Kuramata, K. Sasaki, S. Watanabe, K. Koshi, J. Blevins, O. Bierwagen, S. Krishnamoorthy, K. Leedy, A.R. Arehart, A.T. Neal, S. Mou, S.A. Ringel, A. Kumar, A. Sharma, K. Ghosh, U. Singisetti, W. Li, K. Chabak, K. Liddy, A. Islam, S. Rajan, S. Graham, S. Choi, Z. Cheng, M. Higashiwaki, β-Gallium oxide power electronics, APL Mater 10 (2022) 029201, https://doi.org/10.1063/5.0060327.
[3] M.D. McCluskey, Point defects in Ga_2O_3, J. Appl. Phys. 127 (2020) 101101, https://doi.org/10.1063/1.5142195.
[4] M. Higashiwaki, S. Fujita, Gallium Oxide: Materials Properties, Crystal Growth, and Devices, Springer Nature, Switzerland, 2020.
[5] S. Pearton, F. Ren, M. Mastro, Gallium Oxide: Technology, Devices and Applications, Elsevier, Amsterdam, Netherlands, 2019.
[6] D.V. Lang, Deep-level transient spectroscopy: a new method to characterize traps in semiconductors, J. Appl. Phys. 45 (1974) 3023, https://doi.org/10.1063/1.1663719.
[7] A. Chantre, G. Vincent, D. Bois, Deep-level optical spectroscopy in GaAs, Phys. Rev. B 23 (1981) 5335, https://doi.org/10.1103/PhysRevB.23.5335.
[8] K. Irmscher, Z. Galazka, M. Pietsch, R. Uecker, R. Fornari, Electrical properties of β-Ga_2O_3 single crystals grown by the Czochralski method, J. Appl. Phys. 110 (2011) 063720, https://doi.org/10.1063/1.3642962.
[9] Z. Zhang, E. Farzana, A.R. Arehart, S.A. Ringel, Deep level defects throughout the bandgap of (010) β-Ga_2O_3 detected by optically and thermally stimulated defect spectroscopy, Appl. Phys. Lett. 108 (2016) 052105, https://doi.org/10.1063/1.4941429.
[10] D.L. Losee, Admittance spectroscopy of deep impurity levels: znTe Schottky barriers, Appl. Phys. Lett. 21 (1972) 54, https://doi.org/10.1063/1.1654276.
[11] T. Walter, R. Herberholz, C. Muller, H.W. Schock, Determination of defect distributions from admittance measurements and application to Cu(In,Ga)Se_2 based heterojunctions, J. Appl. Phys. 80 (1996) 4411, https://doi.org/10.1063/1.363401.
[12] S. Paul, R. Lopez, I. Repins, J.V. Li, Study of charge transport properties in a ZnO/CdS/Cu(In,Ga)Se_2 solar cell via admittance spectroscopy, J. Vacuum Sci. Technol. B 26 (2018) 022904, https://doi.org/10.1116/1.5013046.
[13] J.V. Li, J.N. Duenow, D. Kuciauskas, A. Kanevce, R.G. Dhere, M.R. Young, D. H. Levi, Electrical characterization of Cu composition effects in CdS/CdTe thin-film solar cells with a ZnTe:Cu back contact, IEEE J. Photovoltaics 3 (2013) 1095, https://doi.org/10.1109/JPHOTOV.2013.2257919.
[14] H. Okushi, Y. Tokumaru, Isothermal capacitance transient spectroscopy, Jpn. J. Appl. Phys. 20 (1981) 261, https://doi.org/10.7567/JJAPS.20S1.261.
[15] P. Blood, J.W. Orton, The Electrical Characterization of Semiconductors: Majority Carriers and Electron States, Academic Press, London, 1992.
[16] A.T. Neal, S. Mou, S. Rafique, H. Zhao, E. Ahmadi, J.S. Speck, K.T. Stevens, J. D. Blevins, D.B. Thomson, N. Moser, K.D. Chabak, G.H. Jessen, Donors and deep acceptors in β-Ga_2O_3, Appl. Phys. Lett. 113 (2018) 062101, https://doi.org/10.1063/1.5034474.
[17] M.E. Ingebrigtsen, J.B. Varley, A.Yu. Kuznetsov, B.G. Svensson, G. Alfieri, A. Mihaila, U. Badstubner, L. Vines, Iron and intrinsic deep level states in Ga_2O_3, Appl. Phys. Lett. 112 (2018) 042104, https://doi.org/10.1063/1.5020134.
[18] A.Y. Polyakov, N.B. Smirnov, I.V. Shchemerov, A.V. Chernykh, E.B. Yakimov, A. I. Kochkova, A.N. Tereshchenko, S.J. Pearton, ECS J. Solid State Sci. Technol. 8 (2019) Q3091, https://doi.org/10.1149/2.0171907jss.
[19] A.Y. Polyakov, I.H. Lee, N.B. Smirnov, E.B. Yakimov, I.V. Shchemerov, A. V. Chernykh, A.I. Kochkova, A.A. Vasilev, F. Ren, P.H. Carey, S.J. Pearton, Electrical properties, deep levels and luminescence related to Fe in bulk semi-insulating β-Ga_2O_3 doped with Fe, Appl. Phys. Lett. 115 (2019) 032101, https://doi.org/10.1063/1.5108790.

[20] A.T. Neal, S. Mou, R. Lopez, J.V. Li, D.B. Thomson, K.D. Chabak, G.H. Jessen, Incomplete ionization of a 110 meV unintentional donor in β-Ga_2O_3 and its effect on power devices, Sci. Rep. 7 (2017) 13218, https://doi.org/10.1038/s41598-017-13656-x.
[21] H. Ghadi, J.F. McGlone, C.M. Jackson, E. Farzana, Z. Feng, A.F.M. Anhar Uddin Bhuiyan, H. Zhao, A.R. Arehart, S.A. Ringel, Full bandgap defect state characterization of β-Ga_2O_3 grown by metal organic chemical vapor deposition, APL Mater. 8 (2020) 021111, https://doi.org/10.1063/1.5142313.
[22] C.R. DeLeon, A.T. Neal, S. Elhamri, R. Steinbrunner, J. Hendricks, and J. Melnick, Impact of silane flow on donor traps in MOCVD Grown Gallium Oxide, Spring Meeting of the APS Eastern Great Lakes Section (2022). https://meetings.aps.org/Meeting/EGLSS22/Session/C01.3.
[23] J.V. Li, M.H. Wong, Investigation of electric field effect on defects in GaAsN by admittance spectroscopy, Thin Solid Films 758 (2022) 139422, https://doi.org/10.1016/j.tsf.2022.139422.
[24] C.J. Henry, D.V. Lang, Nonradiative capture and recombination by multiphonon emission in GaAs and GaP, Phys. Rev. B 15 (1977) 989, https://doi.org/10.1103/PhysRevB.15.989.
[25] M.E. Ingebrigtsen, L. Vines, G. Alfieri, A. Mihaila, U. Badstubner, B.G. Svensson, A. Kuznetsov, Bulk β-Ga_2O_3 with (010) and (201) surface orientation, Mater. Sci. Forum 897 (2017) 755, https://doi.org/10.4028/www.scientific.net/MSF.897.755.
[26] W. Shockley, Electrons and Holes in Semiconductors with Applications to Transistor Electronics, D. Van Nostrand, New York, 1950.
[27] J.V. Li, X.N. Li, D.S. Albin, D.H. Levi, A method to measure resistivity, mobility, and absorber thickness in thin-film solar cells with application to CdTe devices, Solar Energy Mater. Solar Cells 94 (2010) 2073, https://doi.org/10.1016/j.solmat.2010.06.018.
[28] J.V. Li, D.H. Levi, Determining the defect density of states by temperature derivative admittance spectroscopy, J. Appl. Phys. 109 (2011) 083701, https://doi.org/10.1063/1.3573538.
[29] Y.Y. Lin, A.T. Neal, S. Mou, J.V. Li, Study of defects in β-Ga_2O_3 by isothermal capacitance transient spectroscopy, J. Vacuum Sci. Technol. B 27 (2019) 041204, https://doi.org/10.1116/1.5109088.
[30] S. Duenas, M. Jaraiz, J. Vicente, E. Rubio, L. Ballon, J. Barbolla, Optical admittance spectroscopy: a new method for deep level characterization, J. Appl. Phys. 61 (1987) 2541, https://doi.org/10.1063/1.337930.
[31] J.T. Heath, J.D. Cohen, W.N. Shafarman, Bulk and metastable defects in $CuIn_{1-x}Ga_xSe_2$ thin films using drive-level capacitance profiling, J. Appl. Phys. 95 (2004) 1000, https://doi.org/10.1063/1.1633982.
[32] Z. Kavilova, C. Kurdak, and R.L. Peterson, Observation of impurity band conduction and variable range hopping in heavily doped (010) β-Ga2O3, 34 (2019) 03LT02 10.1088/1361-6641/ab0150.
[33] A.K. Rajapitamahuni, L.R. Thoutam, P. Ranga, S. Krishnamoorthy, B. Jalan, Impurity band conduction in Si-doped β-Ga_2O_3 films, Appl. Phys. Lett. 118 (2021) 072105, https://doi.org/10.1063/5.0031481.
[34] B.I. Shklovskii, A.L. Efros, Electronic Properties of Doped Semiconductors, Springer-Verlag, Berlin, 1984.